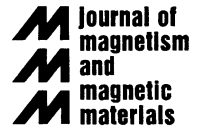




ELSEVIER

Journal of Magnetism and Magnetic Materials 200 (1999) 583–597



www.elsevier.com/locate/jmmm

# Magnetization dynamics in thin films and multilayers

R.E. Camley\*

*Department of Physics, University of Colorado at Colorado Springs, Colorado Springs, CO 80933-7150, USA*

Received 19 January 1999; accepted 8 February 1999

---

## Abstract

The behavior of spin waves is influenced by essentially all the parameters which characterize a magnetic material – exchange interactions, anisotropy, surface effects, dipolar interactions, phase transitions and imperfections. Thus measurements of spin wave frequencies can give important information on characterizing different magnetic materials and structures. In this paper we outline the major results and calculational methods for long-wavelength spin waves in thin films and multilayers. While the primary attention is on ferromagnet-based structures, long-wavelength spin waves in antiferromagnets are also discussed. We indicate how particular measurements of spin wave frequencies can be used to extract the fundamental parameters of the different structures. © 1999 Published by Elsevier Science B.V. All rights reserved.

*Keywords:* Thin films; Multilayers; Magnetization dynamics

---

## 1. Introduction

Why study spin excitations in magnetic materials? There are basically two fundamental reasons:

- (1) All the parameters which characterize the magnetic material – anisotropy, exchange coupling, magnetization, surface effects, impurities, dipolar interactions, and magnetic structure – play a role in determining the frequency of the allowed spin waves. As a result, measurements of spin waves are very useful in determining the fundamental parameters of magnetic structures.
- (2) Spin waves are the fundamental excitations of the magnetic material. As is well known, for

example, they determine the low-temperature behavior of the magnetization. In addition the low-frequency spin waves are excellent indicators of magnetic phase transitions since these transitions are often indicated by a soft mode or by substantial changes in frequency [1–3].

In this paper we will outline the key features of spin waves in thin films and multilayers. We start with a description of the theoretical calculations for long-wavelength spin waves in thick ferromagnetic films and see how this can be used to determine the magnetization and gyromagnetic ratio. These initial calculations are done within a macroscopic basis where the dipolar fields are treated via Maxwell's equations. We then look at thinner films where exchange effects become important and show how spin wave frequencies may be used to determine the exchange coupling in very thin films and the interfilm exchange in magnetic multilayers.

---

\*Tel.: +1-719-2623 512; fax: +1-719-2623013.

E-mail address: rcamley@brain.uccs.edu (R.E. Camley)

For ultrathin films and for systems where the magnetization can change its direction or magnitude from layer to layer a microscopic description of the coupled spin system is more appropriate. Finally, in the last section we outline the calculations for spin waves in antiferromagnets.

Throughout this paper we try to indicate how the properties of the spin waves may be measured and also how these measurements have been used to extract the basic magnetic constants of a particular structure.

## 2. Long-wavelength spin waves in thick ferromagnetic films

As mentioned above, spin wave frequencies are sensitive to many parameters including dipolar fields, magnetization, exchange coupling, anisotropy, and surface conditions. In general this can make calculation of the spin wave frequency a lengthy operation. However, for thick ferromagnetic films there are cases where simple and fundamental analytic expressions can be obtained for the spin wave frequencies. As we shall see below, in this limit it is the dipolar fields which are most important and other contributions may be neglected.

In general one has to calculate the spin motion through the equations of motion which connect the time dependence of the magnetization  $\mathbf{M}$  to the local effective field:

$$\frac{d\mathbf{M}}{dt} = \gamma \mathbf{M} \times \mathbf{H}_{\text{eff}}. \quad (1)$$

For a thick ferromagnet, we can approximate the effective field by a constant external field  $H_0$  in the  $z$  direction and a fluctuating field in an arbitrary direction. This fluctuating field  $\mathbf{h}(t)$  represents the dipolar field and as a result we will eventually have to impose Maxwell's equations to describe this field. Thus we have

$$\frac{d\mathbf{M}(t)}{dt} = \gamma \mathbf{M}(t) \times (\mathbf{H}_0 \hat{z} + \mathbf{h}(t)). \quad (2)$$

One might think that the large exchange field,  $\mathbf{H}_{\text{ex}}$ , would also have to be included. In general this is true, however in the long-wavelength limit the

neighboring spins are all parallel. This means the exchange field is in the same direction as the magnetization since  $\mathbf{H}_{\text{ex}}$  is proportional to  $\mathbf{M}$  in the long-wavelength limit. As a result, the exchange field produces no net torque on the magnetization since  $\mathbf{M} \times \mathbf{H}_{\text{ex}} = 0$ .

We now assume that the magnetization can be separated into a large portion  $\mathbf{M}_s$  pointing along the external field, and a small dynamic portion  $\mathbf{m}(t)$ , i.e.

$$\mathbf{M}(t) = \mathbf{M}_s \hat{z} + \mathbf{m}(t). \quad (3)$$

When Eq. (3) is substituted into Eq. (2) we can connect the dynamic magnetization to the dynamic dipole field  $\mathbf{h}(t)$ . Since we are looking for oscillatory solutions we take all dynamic terms to vary as  $\exp(-i\omega t)$ . Furthermore, we linearize the set of equations by assuming that second-order terms – terms such as  $h_x m_y$  – can be dropped from the equations. After some algebra, we can solve for the dynamic magnetization. This connection can be put in the form of a dynamic susceptibility tensor  $\chi$ :

$$m_x = \chi_{xx} h_x + \chi_{xy} h_y, \quad (4)$$

$$m_y = \chi_{yx} h_x + \chi_{yy} h_y. \quad (5)$$

Using the usual definition  $\mu = 1 + 4\pi\chi$ , we obtain the frequency-dependent permeability. For a simple ferromagnet (with no anisotropies) this has the form

$$\mu(\omega) = \begin{pmatrix} \mu_1 & -i\mu_2 & 0 \\ +i\mu_2 & \mu_1 & 0 \\ 0 & 0 & 1 \end{pmatrix}. \quad (6)$$

The explicit elements of the permeability tensor are given by [4]

$$\mu_1(\omega) = 1 - 4\pi \left( \frac{\gamma^2 M_s H_0}{\omega^2 - \gamma H_0^2} \right), \quad (7)$$

$$\mu_2(\omega) = 4\pi \left( \frac{\gamma \omega M_s}{\omega^2 - \gamma H_0^2} \right). \quad (8)$$

It is worthwhile noting how  $\mu_1$  and  $\mu_2$  behave when the external field,  $H_0$ , is reversed since this will lead to some interesting and important behavior later. Reversing  $H_0$  changes the sign of both  $H_0$  and  $M_s$ . This leaves  $\mu_1$  unchanged and  $\mu_2$  reverses sign. The fact that  $\mu_2$  is odd under a reversal of  $H_0$  eventually leads to interesting nonreciprocal effects.

We now want to learn something about the magnetic waves which can propagate in a magnetic material [5–8]. First imagine the magnetic material is infinite in extent, i.e. we neglect surface effects. We must now solve that static form of Maxwell’s equations

$$\nabla \cdot \mathbf{b} = 0, \tag{9}$$

$$\nabla \times \mathbf{h} = 0 \tag{10}$$

along with constitutive relation

$$\mathbf{b} = \mu \mathbf{h} \tag{11}$$

found earlier. Here, as elsewhere in this paper we use lower case variables to indicate that we are dealing with the fluctuating portions of the various fields. Eq. (10) means that  $\mathbf{h}$  can be found in terms of a magnetic scalar potential, i.e.

$$\mathbf{h} = -\nabla \phi \tag{12}$$

and it will be this scalar potential that we will eventually solve for. Using Eqs. (9)–(12) we find

$$\mu_1 \left( \frac{\partial^2 \phi}{\partial x^2} + \frac{\partial^2 \phi}{\partial y^2} \right) + \frac{\partial^2 \phi}{\partial z^2} = 0. \tag{13}$$

This has the form of an anisotropic Laplace’s equation and is sometimes known as the Walker Equation [6].

Now, we can look for wave-like solutions and see what frequencies are possible. We assume as an example that the scalar potential looks like a bulk wave propagating in the  $xz$  plane. The relationship of the wave vector, coordinate axis and external magnetic field is shown in Fig. 1.

$$\phi(x, y, z, t) = \phi_0(y) e^{i(k_x x + k_z z - \omega t)}. \tag{14}$$

We can change the direction of the wave by choosing different values for  $k_x$  and  $k_z$ . We plug our solution into Eq. (5) and get

$$\mu_1(\omega) = -\left( \frac{k_z}{k_x} \right)^2. \tag{15}$$

Put this in terms of the *direction* or propagation by

$$k_x = k \cos(\theta), \tag{16}$$

$$k_z = k \sin(\theta) \tag{17}$$

and the frequency depends only on the direction of the wave according to

$$\omega = \gamma \sqrt{H_0(H_0 + 4\pi M_s \cos^2 \theta)}. \tag{18}$$

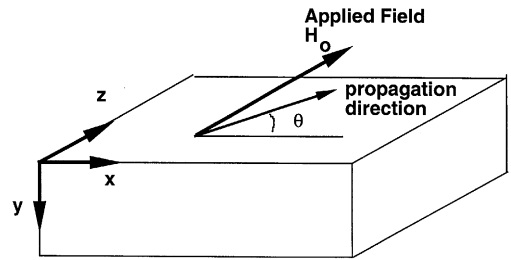


Fig. 1. Thin film geometry. The external field is applied parallel to the surface of the film. The wave propagates at an angle  $q$  with respect to the  $x$ -axis.

Two characteristic frequencies emerge from this equation. The minimum allowed frequency for these bulk waves is  $\gamma H_0$  while the maximum frequency is  $\gamma(H_0 B)^{1/2}$ , where  $B = H_0 + 4\pi M_s$ .

One can also look for bulk and surface waves in the thin film [5]. The geometry for a thin film is illustrated in Fig. 1. Surface waves are characterized by a scalar potential which is composed of a sum of exponentially increasing and decreasing functions within the film and solutions which decay exponentially with distance outside the film. For a film of thickness  $L$  one has:

$$\phi(x, y, z, t) = \phi_a e^{-\alpha y} e^{i(k_x x + k_z z - \omega t)} \quad \text{for } y > L, \tag{19}$$

$$\phi(x, y, z, t) = (\phi_b e^{-\beta y} + \phi_c e^{+\beta y}) e^{i(k_x x + k_z z - \omega t)} \tag{20}$$

for  $y$  inside film,

$$\phi(x, y, z, t) = \phi_d e^{+\alpha y} e^{i(k_x x + k_z z - \omega t)} \quad \text{for } y < 0. \tag{21}$$

When these equations are substituted into the anisotropic Laplace equation, and then the boundary conditions of the continuity of tangential  $H$  and normal  $B$  are imposed at the surfaces of the film, one then finds the implicit dispersion relation for both bulk and surface modes in a thin film. For bulk modes  $\beta$  is imaginary; this results in waves which have a standing wave-like character perpendicular to the surfaces of the film.

The different type of waves which can propagate in the thin film are illustrated schematically in Fig. 2. One particularly interesting feature is that the surface mode is localized at the top or bottom of the film depending on the direction of propagation. We will see later on that this nonreciprocal [9]

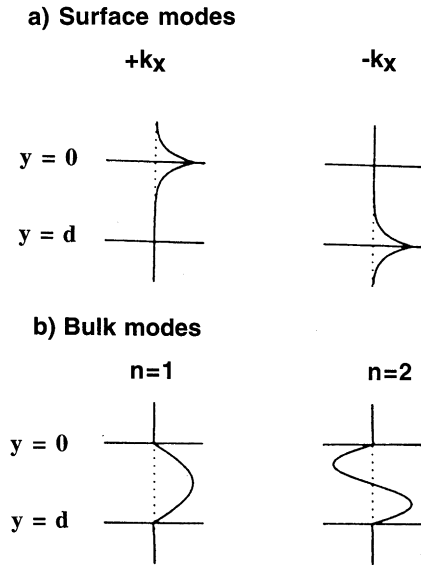


Fig. 2. Illustration of the behavior of the scalar potential as a function of  $y$  for bulk and surface modes in a ferromagnetic film. Note that reversal of the direction of the wave reverses the localization of the surface mode. The film is fairly thick so that  $k_x L = 3$ .

localization is very evident in experimental measurements.

For propagation perpendicular to the applied field, the dispersion relation for surface modes can be put in an explicit form

$$\omega_s = \gamma[(H_0 + 2\pi M_s)^2 - (2\pi M_s)^2 e^{-2|k_x L|}]^{1/2}. \quad (22)$$

Again we note the characteristic limits. For thick films (where the wavelength is much smaller than the thickness of the film) one finds the surface mode frequency has its maximum value  $\omega_s = \gamma(H_0 + 2\pi M_s)$ . For very thin films the surface mode has its minimum value of  $\gamma(H_0 B)^{1/2}$ , which is also the top of the bulk spin wave band.

We pause here to note the utility of the results just developed. For example, the bulk and surface frequencies of a thick film can be measured as a function of applied field in a Brillouin light scattering (BLS) experiment [10–12]. A typical result for an applied field of 3 kG is shown in the inset of Fig. 3. Note that the surface magnon peak (SM) appears on only one side of the spectrum as a result of the nonreciprocal localization discussed earlier. From the peaks seen in the BLS experiment, one

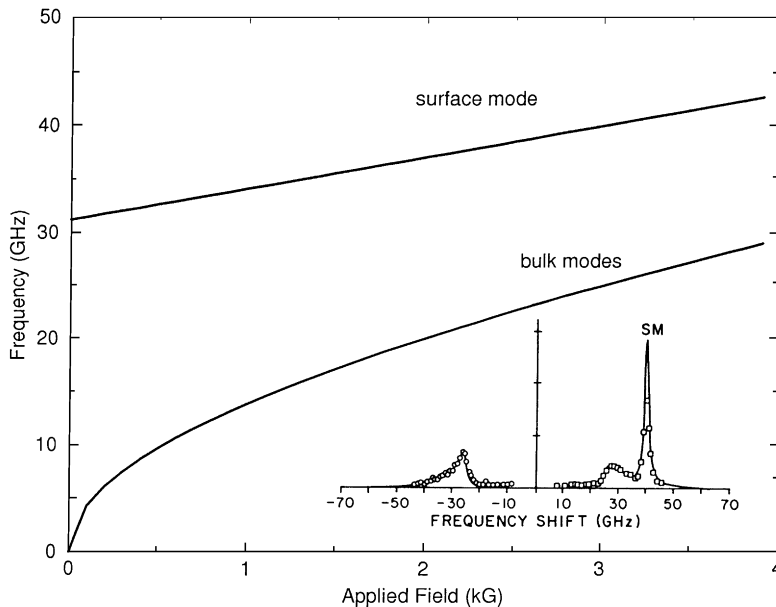


Fig. 3. Frequencies for bulk and surface spin waves as a function of applied magnetic field for a thick ferromagnet. Anisotropies are neglected. The small peaks in the inset are from bulk magnons.

can plot the frequencies of the bulk and surface modes as a function of applied field as seen in Fig. 3. The slope of the surface mode line gives the gyromagnetic ratio  $\gamma$ , and the intercept then gives an absolute measurement for the magnetization!

The treatment above is appropriate for a system with low anisotropy, i.e. permalloy, or for a polycrystalline material. For magnetic materials with strong crystallinity one needs to introduce magnetic anisotropy [13].

### 3. Thin ferromagnetic films

In the development above, we assume that the wavelength of the spin wave was sufficiently long so that every spin was essentially parallel to its neighbor. For thinner films this assumption breaks down for the following reason. As we discussed previously, the bulk modes in a film have the characteristics of standing spin waves, with the effective wavelength perpendicular to the film being on the order of the thickness of the film itself. Thus for thin films the effective wavelength can be quite small and neighboring spins can no longer be parallel.

One way to include the exchange contributions to the effective field is to introduce an effective exchange field [7] in the form of

$$H = D\nabla^2 m, \tag{23}$$

where  $D$  is the exchange stiffness constant. Ultimately, the exchange terms act like an effective external magnetic field acting in the  $z$  direction. The total “external” field is then given by

$$H_{\text{total}} = (H_0 + Dk_y^2)\hat{z}, \tag{24}$$

where  $k_y$  is the component of the wave vector perpendicular to the surfaces of the film.

As an approximation we can thus just replace the  $H_0$  in the dispersion relation by  $H_{\text{total}}$ . The bulk mode frequencies are now given by

$$\omega = \gamma\sqrt{(H_0 + Dk_y^2)(H_0 + Dk_y^2 + 4\pi M_s)}. \tag{25}$$

What values are appropriate for  $k_y$ ? A reasonable approximation is to think of our standing wave

picture in the  $y$  direction. Then

$$k_y = \left(\frac{n\pi}{L}\right) \text{ where } n = 1, 2, 3, \dots \tag{26}$$

We can now make an estimate for a typical value for the exchange field. For Fe  $D = 2.2 \times 10^{-9} \text{ G/cm}^2$ . Suppose  $n = 1$  and  $L = 100 \text{ \AA} = 10^{-6} \text{ cm}$ . Then  $Dk_y^2 = 21.7 \text{ kG}$  which is a substantial contribution to the frequency.

A Brillouin light scattering measurement of the spin wave modes on a thin ferromagnetic film shows a series of standing wave modes [14–16] as is illustrated in Fig. 4. We emphasize that these measurements can be used to characterize the exchange constants and thickness of a ferromagnetic film. Such a measurement is substantially easier than the measurement of spin wave modes in neutron scattering for example, and more direct than an extraction of the exchange constants based on thermal behavior. A collection of data regarding exchange constants is found in Ref. [17].

Although we do not pursue this topic here, BLS and other RF measurement techniques [18–20] such as ferromagnetic resonance have been used to carefully characterize a variety of thin magnetic films. In particular, the bulk and surface anisotropies for thin films can be easily determined through these techniques [21–23].

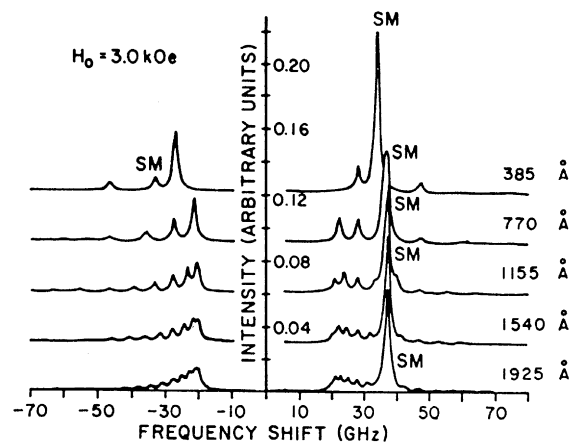


Fig. 4. Calculated Brillouin light scattering spectra for Fe films of different thickness. The small bumps represent scattering from the standing spin waves of different orders.

#### 4. Multilayers – dipolar coupled

Due to advances in the technology of thin film growth, it became possible to fabricate high-quality magnetic multilayer structures in the 1980s. Among the first systems studied experimentally were ones composed of alternating films of ferromagnetic materials and nonmagnetic materials. The nonmagnetic spacer material was generally quite thick (on the order of 200–2000 Å) and as a result there was no direct exchange-like coupling between the ferromagnetic films. The geometry of the multilayer is illustrated in Fig. 5. However, the precessing spins in one ferromagnetic film produce a dipolar field which extends out to influence the motion of spins in other ferromagnetic films.

The spatial extent of the dipolar field is on the order of  $1/\text{wavevector}$ . For spin waves measured with Brillouin light scattering, typical wave vectors have sizes of  $10^5/\text{cm}$  so the dipolar field from one film can extend about 1000 Å. In this case one must solve for the coupled spin wave modes of the entire structure. For a small number of layers, this calculation is very similar to the one presented earlier. One assumes that the magnetic scalar potential in one of the ferromagnetic films can be expressed as a plane wave parallel to the surface and a sum of exponentially increasing and decreasing solutions perpendicular to the surface. Explicitly, one would have

$$\phi(x, y, z, t) = e^{i(k_x x + k_z z - \omega t)} (A_+ e^{+\beta y} + A_- e^{-\beta y}). \quad (27)$$

Similar expressions would hold for the other ferromagnetic films and for the nonmagnetic films. The exponential decay parameters in each region are determined by substituting the expression for  $\phi$  into the anisotropic Laplace equation. The amplitudes ( $A_+$  and  $A_-$  in the example above) for each region are initially unknown. However, by imposing the usual boundary conditions that the tangential components of  $H$  and normal components of  $B$  are continuous one obtains a set of homogeneous equations with the unknown amplitudes as the variables. In order to have a nontrivial solution the determinant of the coefficient matrix must be zero. This condition allows one to find the dispersion relation, i.e. to connect the frequency of the mode,  $\omega$ , to the wave vector  $k$ .

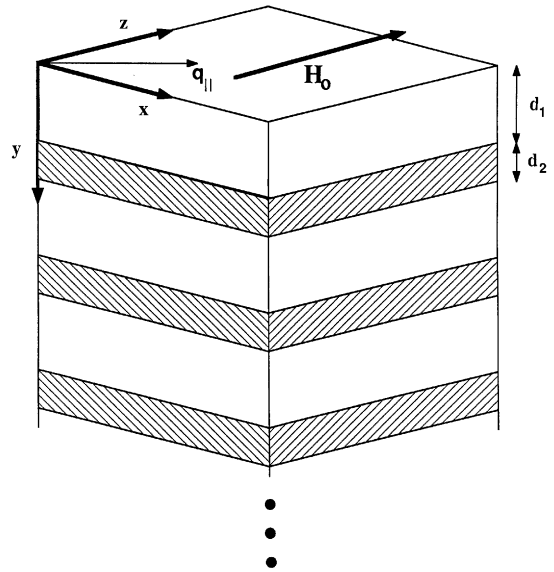


Fig. 5. Superlattice geometry. The thickness of the ferromagnet is  $d_1$  and the thickness of the nonmagnetic spacer is  $d_2$ .

The procedure above can, in principle, be used to find the spin wave modes for an arbitrary multilayer [24]. In practice, it becomes nearly impossible to solve this analytically for more than two ferromagnetic films and for larger structures numerical methods must be used to find the zeros of the determinant. It is therefore of interest to have some sophisticated treatments [25–28].

For a multilayer system with strict periodicity [25,28] the problem of finding the dispersion relation for the collective modes of the entire structure is similar to the problem of the one-dimensional Kronig–Penny model. For the bulk collective modes – the modes in an infinitely extended structure – one seeks solutions for the scalar potential which obey Bloch’s theorem in the direction of periodicity, the  $y$  direction. Thus we expect that the solutions in one unit cell of the periodic structure are related to those in a neighboring cell by a simple phase factor, i.e.

$$\phi(y + L) = e^{i(Q_y L)} \phi(y). \quad (28)$$

Using this assumption to connect the solutions in one unit cell to another, one then imposes the boundary conditions at the interfaces inside the

unit cell and this eventually results in the dispersion relation for the bulk collective modes. The general result is complicated, however a simple result emerges for propagation perpendicular to the applied field and for thin films

$$\omega^2 = \gamma^2 \left( H_0^2 + \frac{4\pi M_s H_0 d_2}{d_1 + d_2} + \frac{4\pi M_s H_0 d_1}{d_1 + d_2} \frac{Q_\perp^2}{Q_\perp^2 + Q_\parallel^2} \right). \quad (29)$$

This gives the frequency as a function of the in-plane propagation wave vector parallel to the layers,  $Q_\parallel$ , and in terms of the wave vector  $Q_\perp$  which governs the phase difference from one unit cell to the next. Here  $d_1$  and  $d_2$  are the thickness of the magnetic and nonmagnetic films, respectively.

For a semi-infinite structure we need to look for solutions for the scalar potential which are localized near the surface of the structure and which decay exponentially as one moves from the top unit cell deeper into the structure. As a result the solutions for the collective surface wave have the form

$$\phi(y + L) = e^{-\alpha L} \phi(y). \quad (30)$$

After application of the boundary conditions for a unit cell one finds the dispersion relation for the surface mode.

It is important to understand the physical nature of the spin wave modes in the superlattice. The collective modes of the entire structure can be composed of bulk modes within each film or of surface modes within each film. This is illustrated in Fig. 6 where we show collective bulk and surface modes which are composed of surface modes in each film.

When the collective mode is composed of surface-type modes in each film, the solution turns out to be remarkably simple

$$\omega = \frac{\gamma}{2} (H_0/\cos \theta + (H_0 + 4\pi M_s)\cos \theta). \quad (31)$$

This is, in fact, just the dispersion relation for a semi-infinite ferromagnet. Thus it almost appears as if the layering plays no role at all. However, this is not true because one finds additionally that the collective surface mode only exists if  $d_1 > d_2$ , i.e. if the ferromagnet film thickness is greater than the

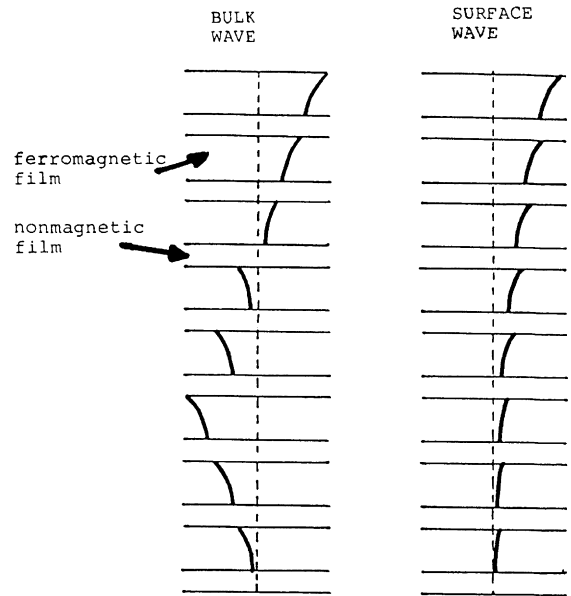


Fig. 6. The scalar potential as a function of position for a collective bulk mode and a collective surface mode. Note that within a film the scalar potential has the characteristics of a surface mode in either case.

thickness of the nonmagnetic material. The dispersion relations for collective bulk and surface modes (composed of surface modes in each film) are illustrated in Fig. 7. Here we see that for  $d_1 > d_2$  a separate surface mode exists at a frequency above the bulk band. The bottom portion of Fig. 7 presents the experimental results [29] which show that a higher frequency mode exists only for  $d_1 > d_2$ . Again we note that the surface mode peak appears on one side of the BLS spectrum.

A variety of other methods have been developed and employed to deal with the dipolar coupled system. These include the effective medium method [30,31] and the transfer-matrix method [32].

### 5. Multilayers – exchange coupled

As we have seen above, two ferromagnetic films separated by a thick nonmagnetic film interact via the long-range dipolar fields. When ferromagnetic films are separated by very thin (5–50 Å) nonmagnetic spacers there can be additional interactions which can be represented

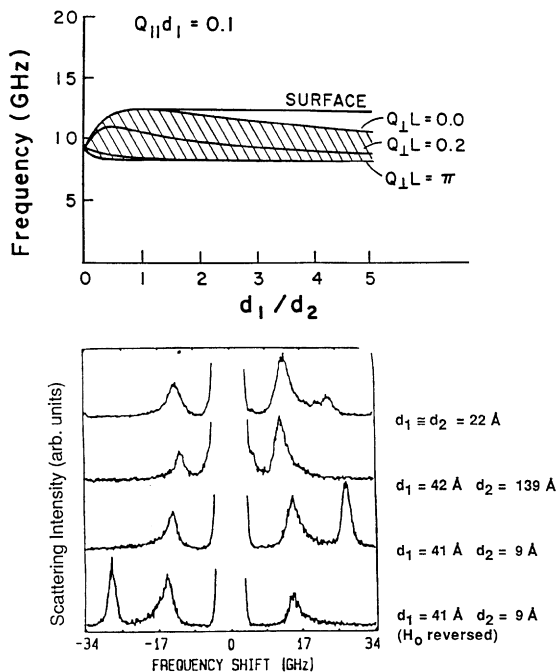


Fig. 7. Top portion shows the dispersion relations for bulk and surface collective modes in a semi-infinite magnetic superlattice as a function of the ratio of the thicknesses of the ferromagnet and the nonmagnetic spacer. The bottom portion shows the experimental BLS spectrum indicating that a surface mode exists for  $d_1/d_2 > 0$  but not for  $d_1/d_2 < 0$ .

mathematically as an effective exchange interaction between the spins at the surfaces of the films. This exchange interaction is thought to arise from a spin polarization of the conduction electrons in the nonmagnetic spacer and depends in part on the thickness of the nonmagnetic film.

A variety of different types of exchange interactions have been observed. First the usual bilinear exchange energy has the form

$$E = -AM_1 \cdot M_2. \quad (32)$$

This represents an effective exchange between the magnetizations in films 1 and 2 with exchange coupling constant  $A$ . If  $A$  is positive the coupling is ferromagnetic in nature while a negative  $A$  indicates antiferromagnetic coupling. In typical systems such as Fe/Cr/Fe [33] or Co/Cu/Co [34] the exchange coupling constant between the ferromag-

netic films oscillates from positive to negative as the thickness of the nonmagnetic film is increased.

In addition to the usual bilinear exchange, a biquadratic form of exchange is sometimes needed to describe the magnetic coupling between the two ferromagnetic films [35]. The biquadratic energy has the form

$$E = -A_2(M_1 \cdot M_2)^2. \quad (33)$$

The key characteristic allowing identification of biquadratic exchange is that the magnetic moments in the two films are neither parallel nor antiparallel to each other in zero field but are at a  $90^\circ$  angle with respect to each other.

Measurements of spin waves are particularly helpful in obtaining reliable values for the interfacial exchange coupling constants. To see this, we use an analogy of two identical pendula coupled by a spring. Each pendulum independently has a fundamental oscillatory mode. When coupled through the spring, two modes for the system emerge. One mode – often known as the acoustic mode – has both pendula moving in phase. As a result the spring is neither compressed or expanded and the frequency of this mode is independent of the coupling. The other mode – the optic mode – has the two pendula moving out of phase and the spring thus plays an important role in determining the frequency of the coupled motion. The same considerations come into play for two coupled ferromagnetic films. If the spin motions in the two films are in phase, the exchange coupling plays no role in the frequency. In contrast, out of phase motion is very sensitive to the interfacial exchange coupling. Fig. 8 shows the behavior of the frequency of the two modes as a function of exchange strength for two exchange-coupled ferromagnetic films [36,37].

This sensitivity to the interfacial coupling can be of great advantage in determining the exchange coupling between ferromagnetic films, and, in fact, this method can be used where other methods fail. As an example consider first two identical ferromagnetic films with antiferromagnetic coupling through the nonmagnetic spacer film. In zero field the magnetizations of the two films are antiparallel and the net magnetization is zero. By applying an external field one can force the magnetizations in

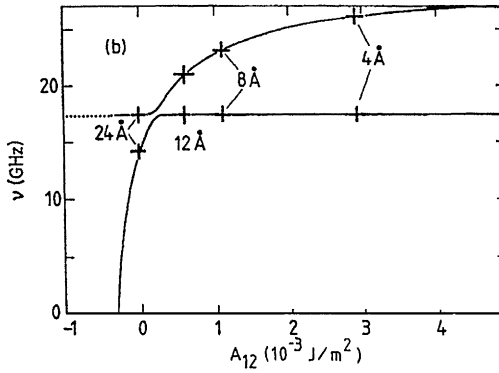


Fig. 8. Frequencies for the acoustic and optic modes in a structure composed of two exchange-coupled permalloy (P) films in a P/Pd/P structure. The experimentally found frequencies for different Pd interlayer thickness are shown with a cross symbol.

the two films to eventually be parallel to the external field and the exchange coupling can then be calculated based on the field necessary for saturation. If however the coupling between the two magnetic films is ferromagnetic in nature, the two magnetizations saturate immediately and this procedure does not work! In contrast, a measurement of the spin wave frequencies, and in particular the out of phase spin wave, gives a good measurement for the effective exchange coupling between films.

The complete calculation for the spin wave modes in dipolar and exchange coupled ferromagnetic films tends to be complex and lengthy and we do not outline these methods here. A number of different schemes have been explored [38–43]. One method is to use a continuum model to describe dipole-exchange spin waves in each ferromagnetic film and then include the interfacial coupling as a boundary condition [38–40]. An effective medium scheme which is appropriate to long wavelength spin waves has also been useful [30,41–43].

### 6. Ultra-thin films and multilayers

Up to now we have discussed methods which are based on a continuum model where the dipolar field could be treated via Maxwell’s equations. When the number of magnetic layers is small, say

2–100 atomic layers, it is more appropriate to deal with the system using a discrete model where each layer is treated independently. In this case one writes down a local energy density appropriate to each layer [44–48]. Schematically, one has

$$E(i) = E_{\text{anisotropy}} + E_{\text{dipolar}} + E_{\text{exchange}} + E_{\text{Zeeman}} \tag{34}$$

The effective field acting on layer *i* is then found through the usual definition

$$\mathbf{H}_{\text{eff}}(i) = - \frac{\partial E(i)}{\partial \mathbf{M}(i)} \tag{35}$$

Then the equation of motion for the magnetization in layer *i* may be written simply as

$$\frac{d\mathbf{M}(i)}{dt} = \gamma(\mathbf{M}(i) \times \mathbf{H}_{\text{eff}}(i)) \tag{36}$$

This is done for each layer in the structure independently. This procedure allows for tremendous flexibility in constructing the system. Surface anisotropies or interfilm exchange fields which act on the outermost layer, for example, are easily included. One may also assume a magnetization which varies in magnitude or direction from layer to layer.

The normal modes of the system may now be calculated straightforwardly. It is assumed that the time dependence of all fluctuating terms is  $\exp(-i\omega t)$ . The coupled set of equations of motion may then be linearized and put in a typical eigenvalue form

$$\begin{pmatrix} M_{11} - i\omega & M_{12} & M_{13} & \cdots & M_{1p} \\ M_{21} & M_{22} - i\omega & M_{23} & \cdots & M_{2p} \\ \cdot & \cdot & \cdot & \cdots & \cdot \\ \cdot & \cdot & \cdot & \cdot & \cdot \\ M_{1p} & M_{2p} & \cdot & \cdots & M_{pp} - i\omega \end{pmatrix} \begin{pmatrix} m_x(1) \\ m_y(1) \\ \cdot \\ m_x(N) \\ m_y(N) \end{pmatrix} = 0 \tag{37}$$

and solved numerically. In Eq. (37) we have assumed that the saturation magnetization in each layer is aligned with the external field along the  $z$ -axis. In that case  $N$  is the total number of magnetic layers and  $p = 2N$ . (For the general case with the magnetization direction varying from layer to layer one would have to include the  $x$ ,  $y$  and  $z$  components of the magnetization in the matrix above and then  $p = 3N$ .) The solution is easily accomplished when the dimension of the matrix is 200 or less, and methods exist for finding the lowest eigenvalues for much larger matrices.

An interesting variation of this method is to use a numerical scheme which calculates the dynamic motion of the spins to first find the equilibrium spin configuration [49] and then the spin wave modes [50]. As above, an effective field approach is used to find the coupled equations of motion for the spins in each layer. The system is then given some initial configuration and allowed to evolve in time according to the equations of motion. As a result of damping, the system evolves to a structure where the spins in each layer are pointing along their local effective field direction. This effectively finds a minimum energy state where the spins in each layer can point in different directions.

The equations of motion for the magnetization in layer  $i$  is now given by

$$\frac{d\mathbf{M}(i)}{dt} = \gamma \mathbf{M}(i) \times \mathbf{H}_{\text{eff}} + \alpha \mathbf{M}(i) \times \dot{\mathbf{M}}(i) \times \mathbf{H}_{\text{eff}}. \quad (38)$$

In the above equation, the first term on the right represents the torque produced on a spin in layer  $i$  by an effective magnetic field. The second term is the Landau–Lifshitz damping term which allows the spin to decay to the local field direction, but keeps the magnitude of the spin constant. Here  $\gamma$  is the gyromagnetic ratio and  $\alpha$  is the effective damping parameter. We note that the dipole field in ultra-thin structures can be treated by including a simple demagnetizing term.

The coupled set of equations is then given an initial state and iterated forward in time through a Runge–Kutta method. The equilibrium position is found by using a large value for the damping constant  $\alpha$ . This forces the system to dynamically relax to the ground state. A small perturbation is

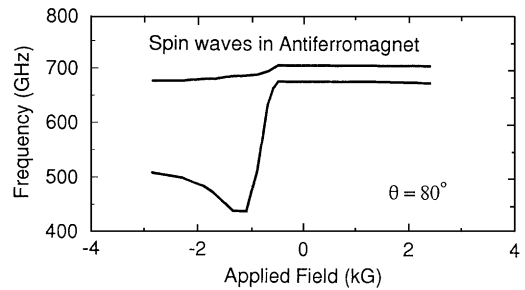


Fig. 9. Frequencies for the two lowest spin wave modes in an antiferromagnet as a function of applied field. As the field is reversed a twist is built into the antiferromagnet and this is where the frequency shows a sharp drop.

then added to the configuration and the time evolution of the spin motion is calculated. The normal mode frequencies are then found by using a Fast Fourier Transform of the time-dependent spin motion.

The method is particularly useful for systems where the magnetization points in slightly different directions in each layer. Recent examples include the calculation [51] of the structure and spin wave modes in a spiral-like structure of Fe/Sm–Co, and the calculation of the structure [50] and spin wave modes [52] in a ferromagnet/antiferromagnet structure which exhibits exchange biasing. As an example we show the calculated frequencies for the fundamental spin wave modes in an antiferromagnet exchange coupled to a ferromagnet in Fig. 9. As the applied field is reversed from its positive value the ferromagnet begins to build a twisted state in the antiferromagnet, and this is reflected in the sudden drop in antiferromagnet spin wave frequencies. This method has also been used to discuss surface phase transitions in Fe/Cr/Fe multilayers with uniaxial anisotropy [53].

## 7. Spin waves in antiferromagnets

The properties of antiferromagnets have recently received renewed attention for a variety of reasons. Many antiferromagnets are insulators and therefore have very different properties from the thoroughly studied ferromagnetic metals of Fe, Ni and

Co. For example, anisotropy fields in antiferromagnets are often in the 100 kG range compared to the 1 kG or less found in the transition metals. Also, antiferromagnets play an important role in the exchange biasing [54] of ferromagnetic films, a feature of current importance in magnetoresistive reading heads [55]. Again in contrast to ferromagnets, antiferromagnets can have long-wavelength spin excitations in the infrared (IR) frequency regime. This makes antiferromagnets of interest for signal processing in the infrared.

In the long-wavelength limit the dynamic properties of a magnetic insulator are governed primarily by the frequency-dependent permeability tensor as we have discussed previously. For an antiferromagnet, a calculation of this tensor begins with the equations of motion for the spins on the two sublattices:

$$\frac{d\mathbf{M}_1}{dt} = \gamma(\mathbf{M}_1 \times \mathbf{H}_1^{\text{eff}}) \quad (39)$$

and

$$\frac{d\mathbf{M}_2}{dt} = \gamma(\mathbf{M}_2 \times \mathbf{H}_2^{\text{eff}}). \quad (40)$$

In the above equations  $\mathbf{M}_1$  and  $\mathbf{M}_2$  are the magnetizations on the two sublattices,  $\gamma$  is the gyromagnetic ratio and  $\mathbf{H}^{\text{eff}}$  is an effective field acting either on sublattice 1 or 2.

The effective field has a number of contributions. For example the effective field acting on sublattice 1 is given by

$$\mathbf{H}_1^{\text{eff}} = \mathbf{H}_1^{\text{exchange}} + \mathbf{H}_1^{\text{anisotropy}} + \mathbf{H}_0 + \mathbf{h}_{\text{dipolar}} \quad (41)$$

with a similar expression for the effective field on sublattice 2. Here  $\mathbf{H}_0$  is the applied field. The exchange field is typically the largest of all the fields above with a magnitude on the order of 100 to 1000 kG. A key point to notice is that the exchange field acting on sublattice 1 comes primarily from the magnetization on sublattice 2, i.e.

$$\mathbf{H}_1^{\text{exchange}} = \lambda\mathbf{M}_2, \quad (42)$$

where  $\lambda$  is the exchange coupling constant. Even in the long-wavelength limit, the two sublattices do not have to be parallel and as a result the large

exchange field produced by sublattice 2 influences the motion of sublattice 1 through Eq. (39).

The large exchange field is a significant difference between the ferromagnet and the antiferromagnet and explains why antiferromagnet excitations lie in the infrared while long-wavelength ferromagnetic spin wave frequencies are in the few GHz region. In the ferromagnet – in the long-wavelength limit – the exchange field is simply proportional to the magnetization:

$$\mathbf{H}^{\text{exchange}} = \lambda\mathbf{M}. \quad (43)$$

As a result the contribution of the exchange field in the equations of motion is zero since  $\mathbf{M} \times \lambda\mathbf{M} = 0$ . So even though the exchange field is very large, it does not influence the motion of the spins. In the antiferromagnet, however, the exchange field does play a role, and the resulting frequencies are much higher.

Using the expressions for the exchange field and any external and anisotropy fields, the coupled equations of motion for the two sublattices can be solved to relate the dipolar driving fields to the fluctuating magnetization. We assume a time dependence of  $\exp(-i\omega t)$  for all the dynamic fields and obtain the frequency-dependent susceptibility tensor defined through the equation

$$\mathbf{M} = \chi(\omega)\mathbf{h}_{\text{dipolar}}. \quad (44)$$

The frequency-dependent permeability is then found through the usual definition

$$\boldsymbol{\mu}(\omega) = 1 + 4\pi\chi(\omega). \quad (45)$$

The explicit form for the permeability can be found in Ref. [56]. Having found the permeability, the electromagnetic modes for the antiferromagnet may be found in the usual way [57]. One looks for wave-like solutions which satisfy Maxwell's equations inside and outside the antiferromagnet. These solutions are then matched using the electromagnetic boundary conditions at the surface of the antiferromagnet, and this results in the dispersion relation. In contrast to the calculations for the ferromagnet, here the frequency is much larger and it is therefore usually appropriate to use the full (retarded) set of Maxwell's equations when calculating the spin modes for the antiferromagnet.

A number of different structures and geometries have been considered theoretically in the literature. Both easy plane and uniaxial antiferromagnets have been studied, and general geometries with arbitrary directions for the applied magnetic field and for the direction of propagation have been examined. Much of this work is summarized in the review article found in Ref. [58].

As an example, consider a geometry where the surface of the antiferromagnet lies in the  $xz$  plane. The results take a particularly simple form for a uniaxial antiferromagnet where the easy axis and the external field are both along the surface and parallel to each other (along the  $z$ -axis), and the direction of propagation is perpendicular to the external field, i.e. in the  $xy$  plane. We look for electromagnetic waves with the electric field parallel to  $z$  and the magnetic field in the  $xy$  plane ( $s$  polarized). With no external field, one may find that the permeability tensor is given by

$$\boldsymbol{\mu}(\omega) = \begin{pmatrix} \mu_1 & 0 & 0 \\ 0 & \mu_1 & 0 \\ 0 & 0 & 1 \end{pmatrix}, \quad (46)$$

where

$$\mu_1(\omega) = 1 + \frac{8\pi H_A M}{\omega_0^2 - \omega^2}. \quad (47)$$

Here  $\omega_0$  is the resonance frequency given by

$$\omega_0 = \gamma[H_A(2H_E + H_A)]^{1/2} \quad (48)$$

and  $M$  is the saturation magnetization of one of the sublattices. In  $\text{FeF}_2$  the anisotropy field  $H_A = 197$  kG and the exchange field  $H_E = 533$  kG and  $M = 0.56$  kG. With a gyromagnetic ratio of  $\gamma = 0.105$   $\text{cm}^{-1}/\text{kG}$  this gives a resonance frequency of  $52.4$   $\text{cm}^{-1}$  or about  $1500$  GHz.

When the applied field is zero the dispersion relations have relatively simple forms. The dispersion relation for the bulk polaritons in zero field is given by the relation

$$k_x^2 + k_y^2 = \varepsilon\mu_1\omega^2/c^2, \quad (49)$$

where  $k_x$  is the component of the wave vector parallel to the surface and  $k_y$  is the wave vector component perpendicular to the surface. The dispersion relation for surface polaritons is given by

an implicit dispersion relation

$$k_x^2 = \left( \frac{\varepsilon - \mu_1}{1 - \mu_1^2} \right) \mu_1 \omega^2 / c^2. \quad (50)$$

The results for the bulk and surface polaritons in  $\text{FeF}_2$  with zero applied field are shown in Fig. 10. We see two frequency regions which represent the bulk excitations. Between the bulk bands we see a surface mode which is reciprocal, i.e. the frequency does not depend on the sign of the wave vector.

A very different dispersion curve is found when there is an external magnetic field as can be seen in Fig. 11. Now there are three bulk bands. While the bulk modes are reciprocal, the surface modes are clearly nonreciprocal. For example one mode which exists at higher frequencies for  $-k_x$  has no counterpart for  $+k_x$  in the same frequency range.

Since these excitations are in the infrared, it is natural to use infrared radiation as a probe. We note that this has been done in the past using a laser at a single frequency [59,60] and also with a FTIR system [61,62]. A particularly effective method is to use the attenuated total reflection (ATR) technique which allows external radiation to couple to the surface modes effectively [63–65].

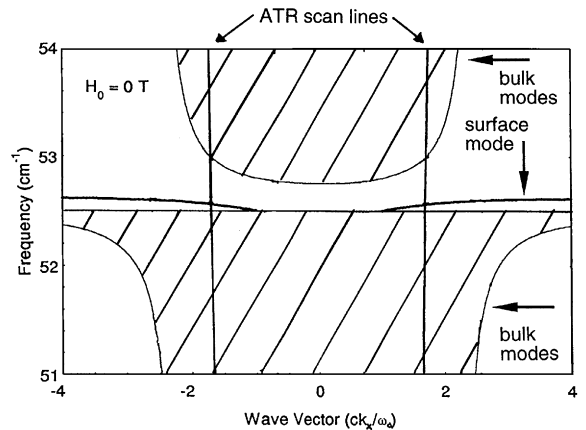


Fig. 10. Calculated dispersion relations for bulk and surface polaritons in  $\text{FeF}_2$ . The frequency,  $\omega/2\pi c$ , is given in wavenumbers. The applied field is zero and so both bulk and surface modes are reciprocal, i.e.  $\omega(+k_x) = \omega(-k_x)$ . Propagation is perpendicular to the easy axis.

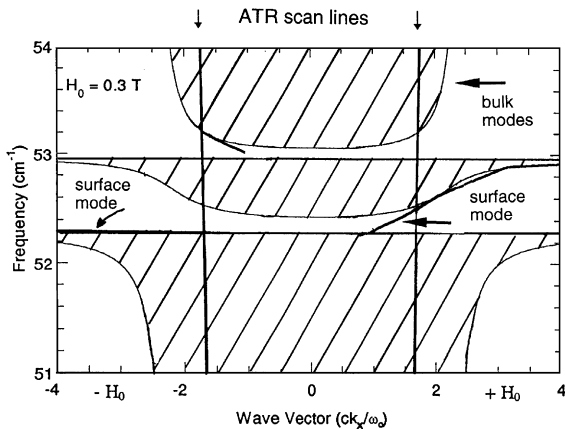


Fig. 11. Dispersion relations for bulk and surface polaritons in  $\text{FeF}_2$  with an applied field of 3 kG. In contrast to the  $H = 0$  case there are now three bulk bands and the surface modes are strongly nonreciprocal.

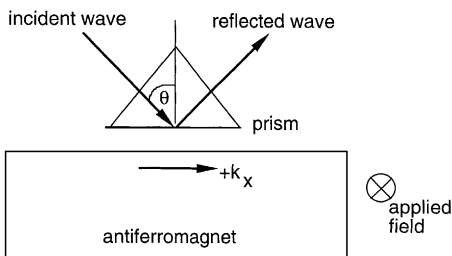


Fig. 12. ATR reflectivity geometry. Reversing the incident and reflected waves reverses the direction of  $k_x$ .

The ATR technique is illustrated in Fig. 12. External light is incident on a Si prism with dielectric constant  $\epsilon = 11.57$ . Because of the high index of the prism, the light is totally internally reflected at the base of the prism and the reflectivity, in the absence of a sample, would be unity. However, there is an evanescent wave below the prism base which can couple to electromagnetic modes in the sample. When this occurs, the reflectivity is reduced from unity since some of the energy is transferred to the sample. A broad region of depressed reflectivity corresponds to the existence of bulk bands, while a sharp dip at one particular frequency corresponds to a surface mode.

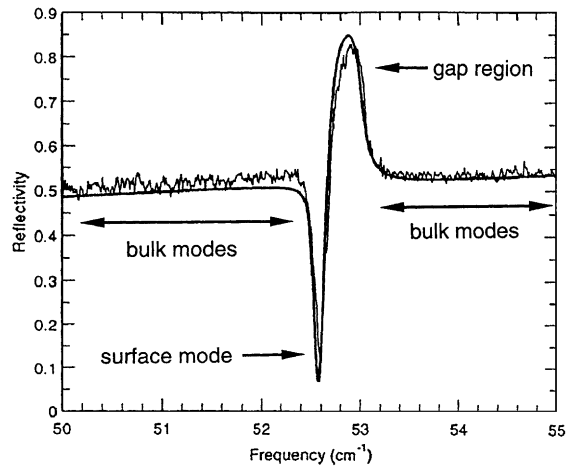


Fig. 13. Experimental and theoretical ATR reflectivity as a function of frequency for  $\text{FeF}_2$  in zero field. The broad regions of depressed reflectivity represent losses to bulk modes. The sharp dip in reflectivity represents the loss to the surface mode. The angle of incidence in the prism is  $30^\circ$  and the gap between the prism and the antiferromagnet is  $17 \mu\text{m}$ .

In Fig. 13 we plot the ATR reflectivity for the case of zero field. The temperature here and in Fig. 14 is 1.7 K. We see in this plot two broad regions of depressed reflectivity corresponding to the two bulk bands of Fig. 10. In between there is a sharp dip in reflectivity, corresponding to the surface mode, and then an increase in reflectivity corresponding to the gap between the bulk modes. It is clear that the experimental results are in very good agreement with both the theoretical calculations for ATR reflectivity and for the dispersion relations calculated in Fig. 10.

In Fig. 14 we again plot ATR reflectivity but now for a field of  $\pm 3$  kG. From the dispersion curve in Fig. 11, we expect a total of three regions of reduced reflectivity corresponding to the three bulk bands. In addition we expect sharper dips representing the surface modes. These features are all present in Fig. 14. A key feature to note is that the surface modes appear at different frequencies depending on the sign of applied magnetic field. This clearly demonstrates the expected nonreciprocity of the surface modes. It may be possible to exploit this nonreciprocity for signal processing in the infrared. For example, the ATR reflectivity near  $52.5 \text{ cm}^{-1}$  is

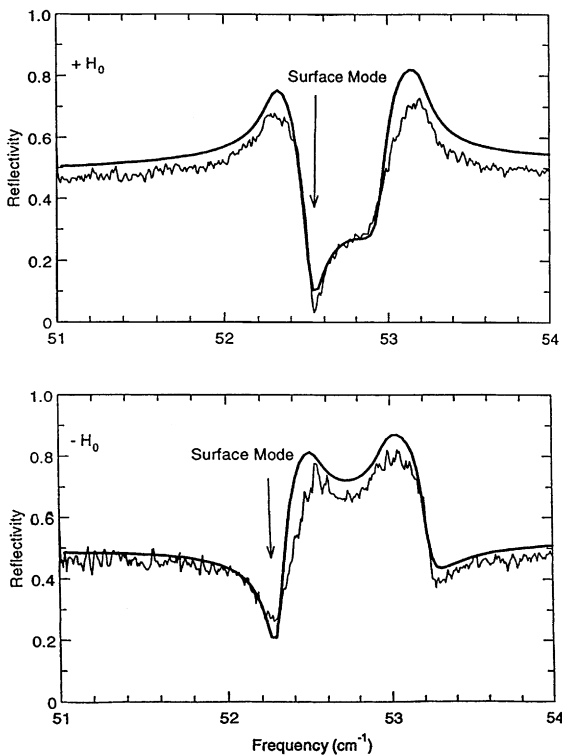


Fig. 14. ATR reflectivity as a function of frequency for  $\text{FeF}_2$  with an applied field of 3 kG. The angle of incidence in the prism is  $30^\circ$  and the gap between the prism and the antiferromagnet is  $17 \mu\text{m}$ . Note the large nonreciprocity in frequency at  $52.5 \text{ cm}^{-1}$ . The smooth curves are the theoretical results and the thinner, jagged lines are the experimental results.

close to zero for positive field. In contrast, the wave travelling in the reversed direction (equivalent to reversing the applied field) has a reflectivity of close to 80%. Thus this system might be used as the basis for a nonreciprocal isolator in the infrared.

### Acknowledgements

This work was supported by US ARO Grant # DAAG55-98-0294

### References

- [1] J.R. Dutcher, J.F. Cochran, I. Jacob, W.F. Egelhoff Jr., *Phys. Rev. B* 39 (1989) 10 430.
- [2] J.F. Cochran, J. Rudd, W.B. Muir, B. Heinrich, Z. Celinski, *Phys. Rev. B* 42 (1990) 508.
- [3] P. Kabos, C.E. Patton, M.O. Dima, D.B. Church, R.L. Stamps, R.E. Camley, *J. Appl. Phys.* 75 (1994) 3553.
- [4] H.A. Morrish, *Physical Principles of Magnetism*, Krieger, Malabar, 1983.
- [5] R.W. Damon, J.R. Eshbach, *J. Phys. Chem. Solids* 19 (1961) 308.
- [6] L.R. Walker, *Phys. Rev.* 105 (1957) 390.
- [7] T. Wolfram, R.E. Dewames, *Prog. Surf. Sci.* 2 (1972) 233.
- [8] M.G. Cottam, D.R. Tilley, *Introduction to Surface and Superlattice Excitations*, Cambridge University Press, Cambridge, 1989.
- [9] See the review article on nonreciprocity by R.E. Camley, *Surf. Sci. Rep.* 7 (1987) 103.
- [10] C.E. Patton, *Phys. Rep.* 103 (1984) 251.
- [11] J.R. Dutcher in: M.G. Cottam (Ed.), *Linear and Non-linear Spin Waves in Magnetic Films and Superlattices* New York, World Scientific, 1994, pp. 287–334.
- [12] J.R. Sandercock, W. Wetling, *J. Appl. Phys.* 50 (1979) 7784.
- [13] G. Rupp, W. Wetling, R.S. Smith, W. Jantz, *J. Magn. Magn. Mater.* 45 (1984) 404.
- [14] R.E. Camley, T.S. Rahman, D.L. Mills, *Phys. Rev. B* 23 (1981) 1226.
- [15] M. Grimsditch, A. Malozemoff, A. Brunsch, *Phys. Rev. Lett.* 43 (1979) 711.
- [16] R.E. Camley, M. Grimsditch, *Phys. Rev. B* 22 (1980) 5420.
- [17] P. Grünberg, in: M. Cardona, G. Güntherodt (Eds.), *Light Scattering in Solids V*, Springer, Berlin, 1989 (Chapter 8) and *Prog. Surf. Sci.* 18 1 (1985).
- [18] J.F. Cochran, in: B. Heinrich, J.A.C. Bland (Eds.), *Ultrathin Magnetic Structures II*, Springer, New York, 1994, p. 222.
- [19] B. Heinrich, in: B. Heinrich, J.A.C. Bland (Eds.), *Ultrathin Magnetic Structures II*, Springer, New York, 1994, pp. 195–290.
- [20] B. Hillebrands, G. Güntherodt, in: J.A.C. Bland, B. Heinrich (Eds.), *Ultrathin Magnetic Structures II*, Springer, Berlin, 1993.
- [21] R.J. Hicken, A. Ercole, S.J. Gray, C. Daboo, J.A.C. Bland, *J. Appl. Phys.* 79 (1996) 4987.
- [22] B. Hillebrands, P. Baumgart, R. Mock, G. Güntherodt, *Phys. Rev. B* 34 (1986) 9000.
- [23] R.L. Stamps, B. Hillebrands, *Phys. Rev. B* 44 (1991) 5095.
- [24] G. Rupp, W. Wetling, W. Jantz, *Appl. Phys. A* 42 (1987) 45.
- [25] R.E. Camley, T.S. Rahman, D.L. Mills, *Phys. Rev. B* 27 (1983) 261.
- [26] P. Grünberg, K. Mika, *Phys. Rev. B* 27 (1983) 2955.
- [27] K. Mika, P. Grünberg, *Phys. Rev. B* 31 (1985) 4465.
- [28] R.E. Camley, M.G. Cottam, *Phys. Rev. B* 35 (1987) 189.
- [29] M. Grimsditch, M.R. Khan, A. Kueny, I.K. Schuller, *Phys. Rev. Lett.* 51 (1983) 498.
- [30] N.S. Almeida, D.L. Mills, *Phys. Rev. B* 37 (1988) 3400.
- [31] N. Raj, D.R. Tilley, *Phys. Rev. B* 36 (1987) 7003.

- [32] J. Barnas, in: M.G. Cottam (Ed.), *Linear and Nonlinear Spin Waves in Magnetic Films and Superlattices*, New York, World Scientific, 1994, 157–206.
- [33] P. Grünberg, R. Schreiber, Y. Pang, M.B. Brodsky, H. Sowers, *Phys. Rev. Lett.* 57 (1986) 2442.
- [34] S.S.P. Parkin, *Phys. Rev. Lett.* 67 (1991) 3598.
- [35] M. Rühlig, R. Schäfer, A. Hubert, R. Mosler, J.A. Wolf, S. Demokritov, P. Grünberg, *Phys. Stat. Solidi A* 125 (1991) 635.
- [36] M. Vohl, J. Barnas, P. Grünberg, *Phys. Rev. B* 39 (1989) 12 003.
- [37] R.L. Stamps, *Phys. Rev. B* 49 (1994) 339.
- [38] B. Hillebrands, *Phys. Rev. B* 41 (1990) 530.
- [39] J. Barnas, *J. Magn. Magn. Mater.* 102 (1991) 319.
- [40] D.L. Mills, *Phys. Rev. B* 45 (1992) 13 100.
- [41] R.L. Stamps, R.E. Camley, *Phys. Rev. B* 54 (1996) 15 200.
- [42] F.C. Noertemann, R.L. Stamps, R.E. Camley, B. Hillebrands, G. Güntherodt, *Phys. Rev. B* 47 (1993) 3225.
- [43] R.J. Aсталos, R.E. Camley, *Phys. Rev. B* 58 (1998) 8646.
- [44] L.L. Hinchey, D.L. Mills, *Phys. Rev. B* 33 (1986) 3329 and 34 (1986) 1689.
- [45] F.C. Noertemann, R.L. Stamps, R.E. Camley, *Phys. Rev. B* 47 (1993) 11 910.
- [46] J.G. LePage, R.E. Camley, *Phys. Rev. Lett* 65 (1990) 1152.
- [47] R.L. Stamps, R.E. Camley, R.J. Hicken, *Phys. Rev. B* 54 (1996) 4159.
- [48] R.P. Erickson, D.L. Mills, *Phys. Rev. B* 44 (1991) 11 825.
- [49] N. Papanicolaou, *Phys. Rev. B* 51 (1995) 15 062.
- [50] R.J. Aсталos, R.E. Camley, *J. Magn. Magn. Mater.*, in press.
- [51] M. Grimsditch, R. Camley, E.E. Fullerton, S. Jiang, S.D. Bader, C.H. Sowers *J. Appl. Phys.* 85 (1999) 5901.
- [52] T. Schulthess, W. Butler, *Phys. Rev. Lett.* 81 (1998) 4516.
- [53] S. Rakhmanova, D.L. Mills, E.E. Fullerton. *Phys. Rev. B* 57 (1998) 476.
- [54] J. Nogues, D. Lederman, T.J. Moran, I.K. Schuller, *Phys. Rev. Lett.* 76 (1996) 4624.
- [55] K.M.H. Lenssen, A.E.M. De Veirman, J.J.T.M. Donkers, *J. Appl. Phys.* 81 (1997) 4915.
- [56] D.L. Mills, E. Burstein, *Rep. Prog. Phys.* 37 (1974) 817.
- [57] R.E. Camley, D.L. Mills, *Phys. Rev. B* 26 (1982) 1280.
- [58] K. Abraha, D.R. Tilley, *Surf. Sci. Rep.* 24 (1996) 129.
- [59] L. Remer, B. Lüthi, H. Sauer, R. Geick, R.E. Camley, *Phys. Rev Lett.* 56 (1986) 2752.
- [60] R.W. Sanders, D. Pagnette, V. Jaccarino, S.M. Rezende, *Phys. Rev. B* 10 (1974) 132.
- [61] R.C. Ohlmann, M. Tinkham, *Phys. Rev.* 123 (1961) 425.
- [62] T. Dumelow, D. Brown, T.J. Parker, 18th International Conference on Millimeter Waves, Colchester, *Proc. SPIE* 2104 (1993) 633.
- [63] M.R.F. Jensen, T.J. Parker, K. Abraha, D.R. Tilley, *Phys. Rev. Lett* 75 (1995) 3756.
- [64] M.R.F. Jensen, S.A. Feiven, T.J. Parker, R.E. Camley, *Phys. Rev. B* 55 (1997) 2745.
- [65] M.R.F. Jensen, S.A. Feiven, T.J. Parker, R.E. Camley, *J. Phys: Condens Matter* 9 (1997) 7233.